crystals

MDPI

Article

Effect of Fe_2O_3 on Electro-Deoxidation in Fe_2O_3-Al_2O_3-NaCl-KCl System

Yanke Xu, Hongyan Yan *, Zhenwei Jing, Xiwei Qi, Hui Li and Jinglong Liang

College of Metallurgy and Energy, North China University of Science and Technology, Tangshan 063210, China; 15032500323@163.com (Y.X.); jzw18251629319@163.com (Z.J.); qixiwei@ncst.edu.cn (X.Q.); lh@ncst.edu.cn (H.L.); ljl@ncst.edu.cn (J.L.)

* Correspondence: yanhy@ncst.edu.cn

Abstract: The reduction of Fe_2O_3-Al_2O_3 is one of the important reactions in the resource utilization of iron-containing oxide waste. Fe_2O_3-Al_2O_3 was electro-deoxidized in the NaCl-KCl system by molten salt electrolysis to prepare FeO/Al_2O_3. The effect of the Fe_2O_3 content on the electro-deoxidation reaction process was studied. The results show that under the conditions of 850 °C, 2.3 V, and electro-deoxidation for 4 h, FeO/Al_2O_3 could be obtained by controlling the content of Fe_2O_3. The deoxidation process was divided into three stages: electric double layer charging, Fe_2O_3 electro-deoxidation to Fe_3O_4, and Fe_3O_4 electro-deoxidation to FeO. With the increase in the Fe_2O_3 content, the deoxidation reaction rate increased, and the low-valence iron oxide particles obtained by electro-deoxidation became larger. The mechanism of the influence of Fe_2O_3 on the electro-deoxygenation process was determined by analyzing the experimental results. The increase in the Fe_2O_3 content increased the concentration of activated molecules in the system, while it reduced the resistance of electro-deoxidation. The migration of active particles in the cathode was smoother, which increased the percentage of deoxygenation of activated molecules, thereby shortening the process of the deoxidation reaction.

Keywords: molten salt electrolysis; Fe_2O_3-Al_2O_3-NaCl-KCl system; FeO/Al_2O_3; Fe_2O_3 influence mechanism

Citation: Xu, Y.; Yan, H.; Jing, Z.; Qi, X.; Li, H.; Liang, J. Effect of Fe_2O_3 on Electro-Deoxidation in Fe_2O_3-Al_2O_3-NaCl-KCl System. *Crystals* **2021**, *11*, 1026. https://doi.org/10.3390/cryst11091026

Academic Editor: Heike Lorenz

Received: 7 August 2021
Accepted: 24 August 2021
Published: 26 August 2021

1. Introduction

Fe_2O_3 and Al_2O_3 are the main components of solid waste such as red mud, blast furnace slag, and zinc kiln slag [1–3]. In order to treat these solid wastes as resources, researchers have reduced Fe_2O_3 to low-valent FeO or Fe_3O_4 through fire and wet methods and finally obtained metallic iron [4,5], ferroalloys [6], roadbed materials [7], and Fe-$FeAl_2O_4$ composite materials [3,8,9]. Therefore, the reduction reaction of the Fe_2O_3-Al_2O_3 system is an important reaction to realize the resource treatment of solid waste, and research on the system reaction is of great significance.

At present, the reduction reaction of the Fe_2O_3-Al_2O_3 system is mainly through C reduction [10,11], H_2 reduction [12,13], CO reduction [14], and CO-CO_2 [15] reduction. These methods have high energy consumption and CO_2 emission problems. In recent years, the widely used molten salt electrolysis method has been used as a typical electrochemical method with low energy consumption and no CO_2 emissions. It mainly includes the FFC method [16], the SOM method [17], the OS calcium thermal method [18], and the USTB method [19]. Through molten salt electrolysis, high-melting point metals, metal alloys, intermetallic compounds, and carbide ceramics were prepared in molten salt systems such as $CaCl_2$-NaCl and NaCl-KCl [20]. Electro-deoxidation research on the Fe_2O_3-Al_2O_3 system mainly focused on the preparation of FeAl and its intermetallic compounds [21–24], while the intermediate product FeO-Al_2O_3 has received fewer reports. The reduction reaction of Fe_2O_3-Al_2O_3 to FeO-Al_2O_3 is a necessary process for the reduction of Fe_2O_3-Al_2O_3 to

metal Fe, FeAl, or its intermetallic compounds. It is one of the key links to obtaining the reduction mechanism of Fe_2O_3-Al_2O_3.

Herein, reduction of Fe_2O_3-Al_2O_3 to FeO-Al_2O_3 was studied by using molten salt electrolysis at 850 °C in a NaCl-KCl melt. The microstructure and phase composition of the deoxygenated products were examined by using SEM and XRD. By examining the changes in the composition and structure of the cathode during the electrolysis process, the influence law of the Fe_2O_3 content on the electrolysis process and the electrosynthesis pathway of FeO-Al_2O_3 in molten salt were also studied.

2. Experimental

The raw materials in this experiment, namely, pure Al_2O_3 (Macklin Group Co., Ltd., Shanghai, China, Analytical reagent) and Fe_2O_3 (Sinopharm Group Co., Ltd., Shanghai, China, Analytical reagent) powders, were used as the cathode precursors. First, the amounts of Al_2O_3 and Fe_2O_3 were ball milled in ethanol for 6 h according to the mass ratio in Table 1. Then, the slurry was vacuum dried for 4 h, and the powder mixture was pressed into cylindrical pellets ($10 \times 3 \times 1$ mm^3) under a uniaxial pressure of 8 MPa. The pellets were sintered at 800 °C for 4 h under argon flow to obtain cathode pellets. Then, the cathode pellets were connected to a 304 stainless-steel wire to assemble the cathode. A high-density graphite sheet ($100 \times 15 \times 5$ mm^3) served as the anode. A eutectic mixture of NaCl-KCl (NaCl/KCl = 50.6:49.4 mol %, Sinopharm Group Co., Ltd., Shanghai, China, Analytical reagent) was used as the electrolyte, which was packed in a graphite crucible and dehydrated at 300 °C for 24 h. The graphite crucible, filled with the mixed salt, was introduced into the bottom of a tube furnace. Then, the furnace was sealed, and ultra-high purity argon gas was flushed into the reactor to provide a protective atmosphere. The furnace temperature was increased to 850 °C under continuous argon circulation. Then, a fresh graphite sheet and cathode were lowered into the melt. The electrolysis was carried out at 2.3 V for 4 h. After electrolysis, the samples were carefully rinsed with distilled water several times to remove the adhering salt and immersed in distilled water for 12 h, followed by drying at 150 °C for 0.5 h. The schematic illustration of the electrochemical deoxidation is shown in Figure 1.

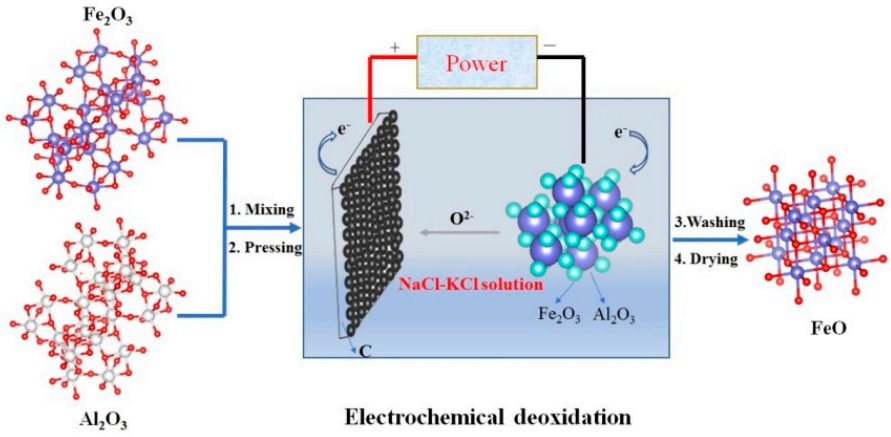

Figure 1. Schematic illustration of the electrochemical deoxidation strategy of Fe_2O_3/Al_2O_3.

Table 1. Specific experimental conditions in electrochemical deoxidation.

Samples	*E* (Decomposition Voltage) V	*T* (Temperature) °C	*t* (Reaction Time) h	mFe_2O_3/mAl_2O_3
S_1	2.3	850	4	1:1
S_2	2.3	850	4	3:2
S_3	2.3	850	4	2:1
S_4	2.3	850	4	4:1
S_5	2.3	850	0.5	3:2
S_6	2.3	850	1	3:2

The phase composition was identified by using X-ray diffraction (XRD, XPert PRO MPD, PANalytical, Almelo, The Netherlands). The microstructure and element analyses were carried out with SEM and EDS (GeminiSEM 300, Zeiss, Germany), respectively.

3. Results and Discussion

3.1. Thermodynamic Analysis and Electrochemical Reduction of Fe_2O_3-Al_2O_3

When energized, the Al_2O_3 and Fe_2O_3 in the molten salt would undergo the following electrolysis reactions:

$$Al_2O_3(s) = 2Al(s) + 2/3O_2(g) \quad (1)$$

$$Fe_2O_3(s) = 2/3Fe_3O_4 + 1/6O_2(g) \quad (2)$$

$$Fe_3O_4(s) = 3FeO + 1/2O_2(g) \quad (3)$$

$$FeO(s) = Fe + 1/2O_2(g) \quad (4)$$

The standard Gibbs free energy of the possible reaction of Fe_2O_3 and Al_2O_3 in the molten salt system at different temperatures could be calculated by using FactSage7.3. The standard theoretical decomposition voltage E^{Θ} was calculated by Formula (5).

$$\Delta G^{\Theta} = -nFE^{\Theta} \quad (5)$$

where ΔG^{Θ} is the standard Gibbs free energy (kJ·mol^{-1}); E^{Θ} is the theoretical decomposition voltage in the standard state (V); F is the Faraday constant (96,485 C·mol^{-1}); and n is the number of electrons gained or lost in the reaction equation.

Figure 2 shows the change curve of E^{Θ} with T in different reactions. As the reaction temperature increases, E^{Θ} becomes more positive. At 600~1100 °C, the order of reaction among (1)~(4) is (2) > (3) > (4) > (1).

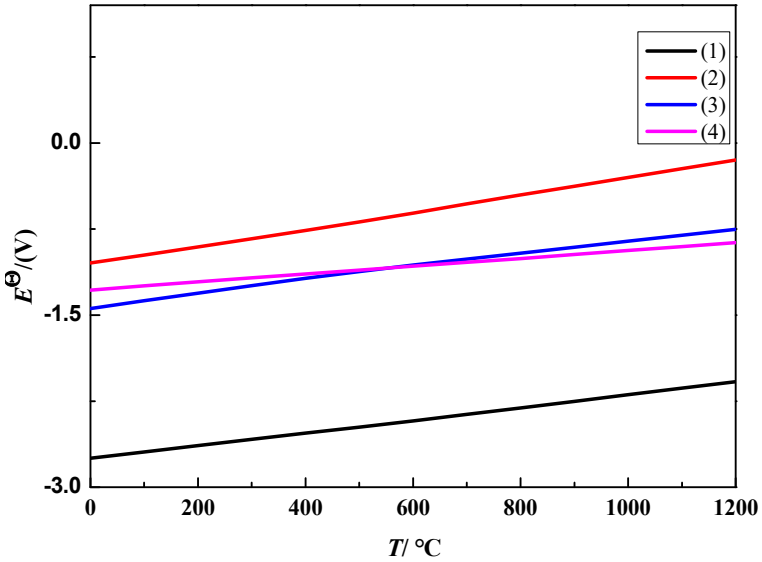

Figure 2. E^{Θ}–T diagram of electrochemical reactions that may occur in the process of electro-deoxidation.

3.2. Effect on Deoxygenation Rate

Figure 3 shows the XRD pattern of the electrolysis under the experimental conditions in Table 1. The Fe_2O_3 content in the S_1~S_4 samples increased sequentially. S_1 and S_2 electrolyzed to Fe_3O_4, FeO, and Al_2O_3. S_3 and S_4 electrolyzed to FeO and Al_2O_3. The peaks of Fe_3O_4 gradually weakened from S_1 to S_4, the peaks of FeO became stronger, and the peaks of Al_2O_3 became weaker in turn. These experimental results show that with the increase in the Fe_2O_3 content, it was easier for FeO to be formed, and Al_2O_3 appeared to be reduced to a certain extent. This change of FeO was due to the increase in Fe_2O_3 in the samples. It increased the mass percentage of Fe_2O_3 activated molecules in the system that

could participate in the electrical deoxidation reaction, thereby increasing the deoxidation reaction rate. As the external field conditions such as the temperature and voltage of the molten salt system had not changed, the diffusion flux of O^{2-} in the NaCl-KCl molten salt remained unchanged. As the deoxidation reaction rate increased, the O^{2-} produced by electrolysis could not be delivered to the anode in time, and more O^{2-} accumulated near the cathode. This part of O^{2-} reacted with Na^+ and K^+ to generate Na_2O and K_2O, and then it reacted with Al_2O_3 to generate $NaAlO_2$ and $KAlO_2$. As $NaAlO_2$ and $KAlO_2$ dissolved in the NaCl-KCl molten salt, this resulted in a decrease in Al_2O_3 in the cathode. The electrochemical reaction of Fe_2O_3 consisted of two steps. The first reaction electrolyzed to Fe_3O_4, and then the reaction of Fe_3O_4 electrolyzed to FeO. This conclusion is consistent with literature reports [21,25,26].

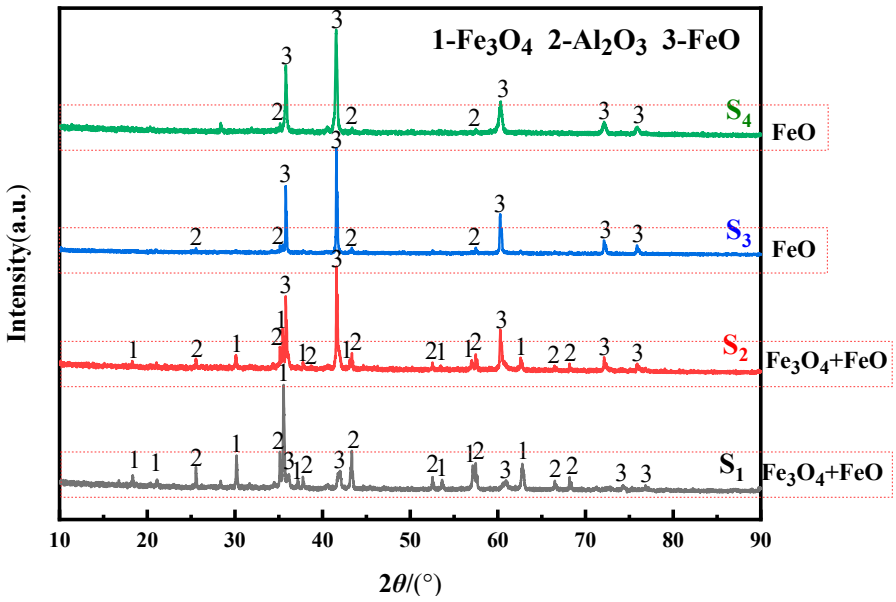

Figure 3. XRD patterns of oxide electrolysis products with different raw material ratios.

Figure 4 shows the change curves of the current with time in the process of S_1~S_4 electric deoxidation. The current is the amount of electricity per unit area, and it represents the rate of electrical deoxidation during the process of electrical deoxidation. The Fe_2O_3/Al_2O_3 electro-deoxygenation reaction process was divided into three stages: A, B, and C. Stage A was the charging process of the electric double layer. The current increased with time and reached the maximum current. At this time, the resistance was the smallest, the electric deoxidation rate was the highest, and the current was the largest, and the most active particles were produced. When the current reached the maximum current, this indicated that the electric double layer had been fully charged, and the electrical deoxidation reaction began to occur at 3PIs. Stage B was the Fe_2O_3 electro-deoxidation reaction process. Combined with the results of Figure 3, this stage should be the reaction of Fe_2O_3 electro-deoxidation to Fe_3O_4 (i.e., reaction (2)), and the current decreased with the reaction time. As the electric deoxidation of Fe_2O_3 to Fe_3O_4 progressed, the molten salt passed through the product layer and formed new 3PIs at the reaction product/unreacted material. The Fe^{3+} active particles obtained electrons at the 3PIs, and O^{2-} diffused into the NaCl-KCl molten salt and migrated to the anode. As with the above-mentioned Fe_2O_3 electro-deoxygenation to Fe_3O_4 reaction, 3PIs formation, O^{2-} transmission, and other reaction processes would increase the resistance of the system, and the current would decrease with time. Stage C was the process of Fe_2O_3 electro-deoxygenation to FeO (i.e., reactions (2) and (3)). The current decreased with the reaction time and was smaller than that in stage B. Compared with stage B, stage C increased the reaction of Fe_3O_4 electro-deoxidation to FeO (i.e., reaction (3)), and the resistance of the system further increased, meaning the current decreased with time and was less than the phenomenon of the stage B current.

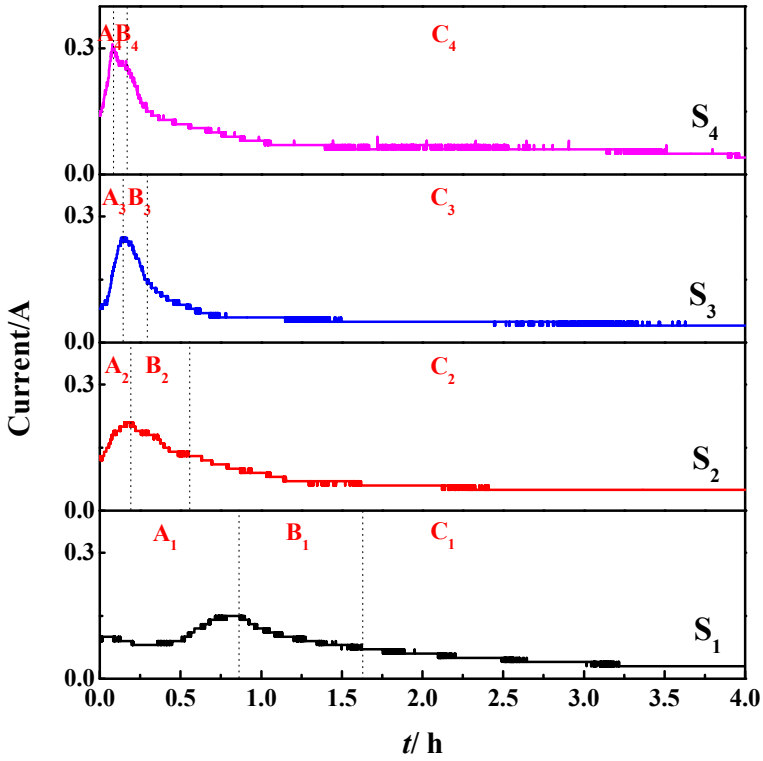

Figure 4. The current–time curves during electrolysis of S_1 (mFe_2O_3/mAl_2O_3 = 1:1), S_2 (mFe_2O_3/mAl_2O_3 = 3:2), S_3 (mFe_2O_3/mAl_2O_3 = 2:1), and S_4 (mFe_2O_3/mAl_2O_3 = 4:1) at 2.3 V, 850 °C, and 4 h.

For the *I*–*t* curves corresponding to S_1, S_2, S_3, and S_4, it was found that stage A, stage B, and stage C had certain changes. In stage A, the slopes of the corresponding curves for S_1~S_4 became larger, and the time to complete the electric double layer charging process was 0.78 h, 0.19 h, 0.16 h, and 0.09 h, which shows a gradual decrease, and the maximum current was 0.15A, 0.20 A, 0.24 A, and 0.3 A, which shows a gradual increase. Similarly, in stage B and stage C, the slopes of the corresponding curves of S_1~S_4 became larger, and the time required to complete the reaction of this stage became shorter. These results show that the rate of Fe_2O_3/Al_2O_3 electric deoxidation increased with the increase in the Fe_2O_3 content. It promoted the progress of the electric deoxidation reaction and shortened the time required to complete the corresponding reaction process. There are two reasons for the above phenomenon. One is that the increase in Fe_2O_3 increased the number of Fe_2O_3 activated molecules in the system that could participate in the electro-deoxygenation reaction. This increased the initial concentration of activated molecules in the Fe_2O_3 electro-deoxygenation reaction, thereby increasing the deoxygenation reaction rate. The second is that Al_2O_3 is an oxide with high resistivity and strong electrical insulation [27]. Al_2O_3 in the S_1~S_4 samples decreased sequentially. This meant that the resistance of the deoxidizing system decreased correspondingly and reduced the resistance of the free electrons to 3PIs. In turn, the deoxygenation reaction rate was increased. The effect of the Fe_2O_3 content on the deoxidation rate is consistent with the XRD results in Figure 3.

3.3. Effect on Organizational Structure

Figures 5–7 showed the SEM morphology, spot scan, and surface scan of the Fe_2O_3/Al_2O_3 electro-deoxidation product. It can be seen that S_1 and S_2 are Fe_3O_4, FeO, and Al_2O_3. S_3 and S_4 are FeO and Al_2O_3. Al_2O_3 is the regular and smooth large particles, and the Fe_3O_4 and FeO particles are smaller. Fe_3O_4 and FeO adhered to Al_2O_3, nucleated, and grew. With the increase in the Fe_2O_3 content, the exposed Al_2O_3 decreased, and the low-valence iron oxides surrounding the surface of the Al_2O_3 particles increased. The low-valence

iron oxide particles gradually became larger and angular polyhedrons. Under the same electrolysis conditions, with the increase in the Fe_2O_3 content, a low content of Fe_2O_3 could produce Fe_3O_4 and FeO, while a high content only produced FeO. This indicates that the increase in the Fe_2O_3 content increased the deoxidation reaction rate. The large, smooth, high-resistivity Al_2O_3 particles hindered the migration of active particles in the deoxidation process. Active particles needed to bypass Al_2O_3 and undergo the electrical deoxidation reaction on the Fe_2O_3 around Al_2O_3. Therefore, the Fe_3O_4 and FeO particles grew around Al_2O_3, and the decrease in the Al_2O_3 content was also beneficial to increase the deoxidation reaction rate. With the increase in the electro-deoxidation rate, the process of Fe_2O_3 electro-deoxidation to Fe_3O_4 (reaction (2)) was shortened, and the reaction of Fe_3O_4 electro-deoxidation to FeO (reaction (3)) was faster. At the same time, the FeO crystal nucleus had more time to grow, finally obtaining larger FeO particles.

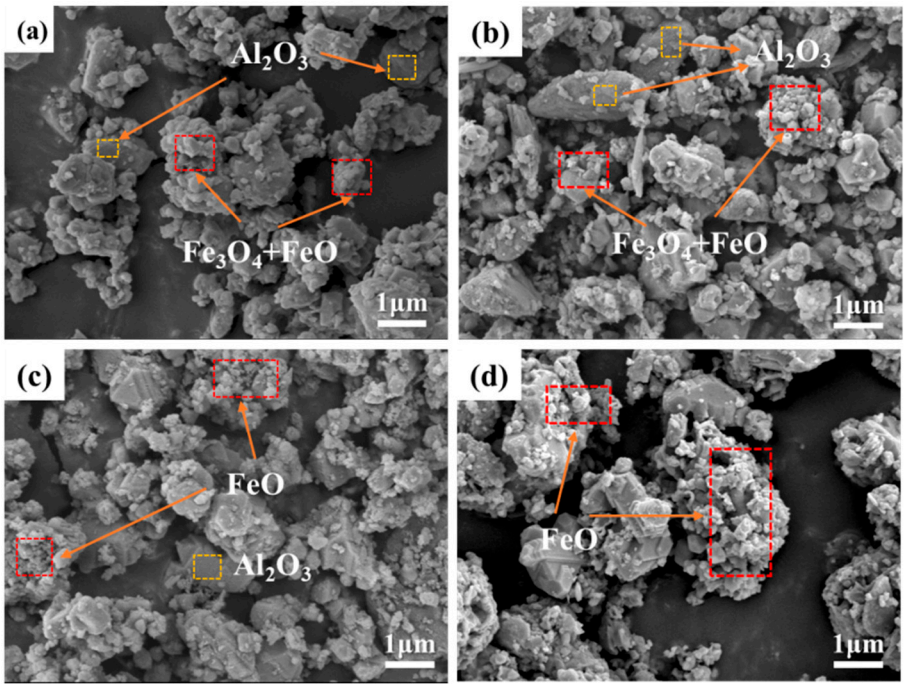

Figure 5. The SEM images of S_1 (mFe_2O_3/mAl_2O_3 = 1:1) in (**a**), S_2 (mFe_2O_3/mAl_2O_3 = 3:2) in (**b**), S_3 (mFe_2O_3/mAl_2O_3 = 2:1) in (**c**), and S_4 (mFe_2O_3/mAl_2O_3 = 4:1) in (**d**) at 2.3 V, 850 °C, and 4 h.

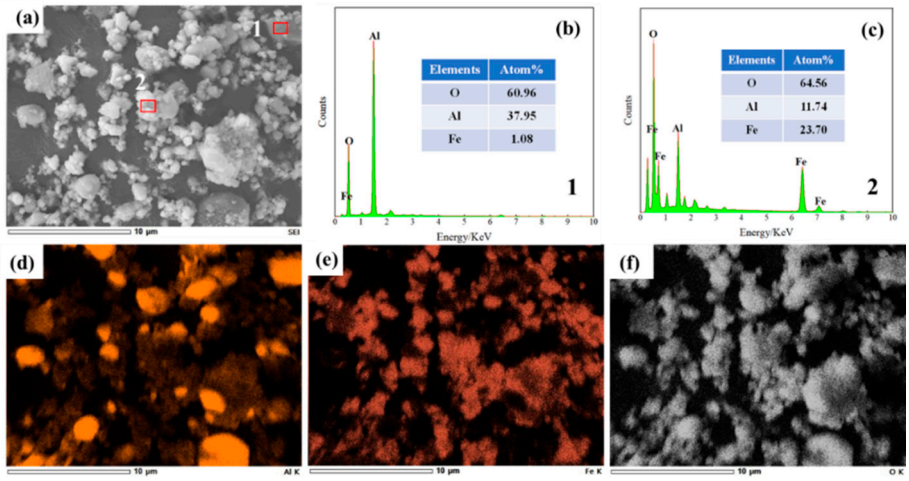

Figure 6. The SEM images of S_1 (mFe_2O_3/mAl_2O_3 = 1:1) in (**a**), point spectrum for 1 in (**b**), point spectrum for 2 in (**c**), and the EDS spectrum of Fe in (**d**), Al in (**e**), and O in (**f**) at 2.3 V, 850 °C, and 4 h.

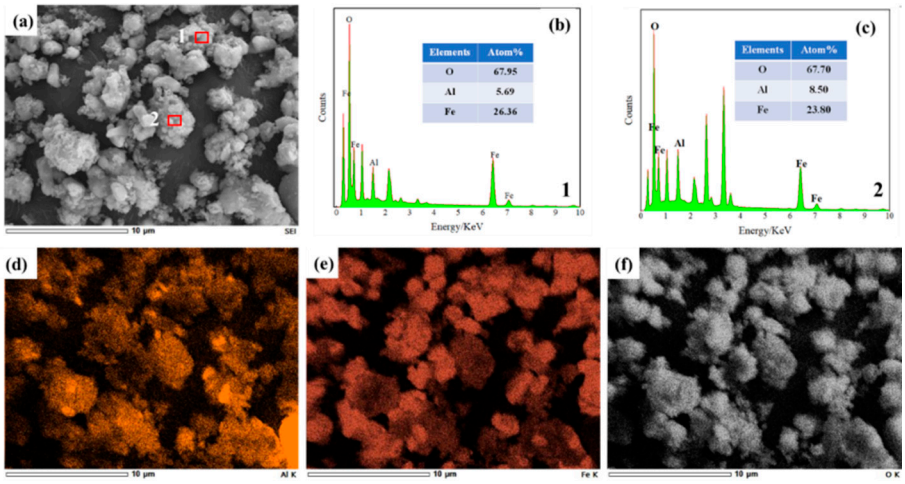

Figure 7. The SEM images of S_4 (mFe_2O_3/mAl_2O_3 = 4:1) in (**a**), point spectrum for 1 in (**b**), point spectrum for 2 in (**c**), and the EDS spectrum of Fe in (**d**), Al in (**e**), and O in (**f**) at 2.3 V, 850 °C, and 4 h.

3.4. Effect Mechanism

From the above XRD and SEM results, it can be seen that the increase in the Fe_2O_3 content increased the deoxidation reaction rate of FeO/Al_2O_3 prepared by Fe_2O_3/Al_2O_3 electro-deoxidation. In order to further clarify the deoxygenation reaction process, XRD analysis was performed on the deoxygenation products of S_2 at 0.5 h, 1 h, and 4 h, as shown in Figure 8. When the reaction reached 0.5 h, the sample color changed from red to black (Figure 9), and the deoxidation product was Fe_3O_4 and Al_2O_3. When the reaction reached 1 h, the deoxidation product was Fe_3O_4, FeO, and Al_2O_3. When the reaction reached 4 h, the sample color changed from black to dark green (Figure 9), and the deoxidized product was also Fe_3O_4, FeO, and Al_2O_3.

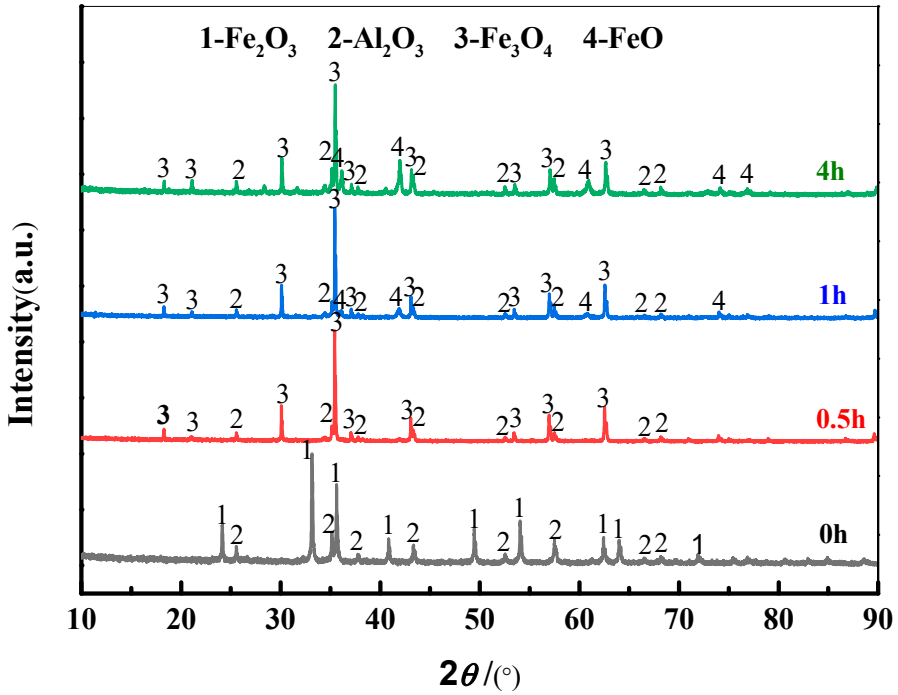

Figure 8. XRD patterns of S_2 (mFe_2O_3/mAl_2O_3 = 3:2, at 2.3 V, 850 °C) at different times.

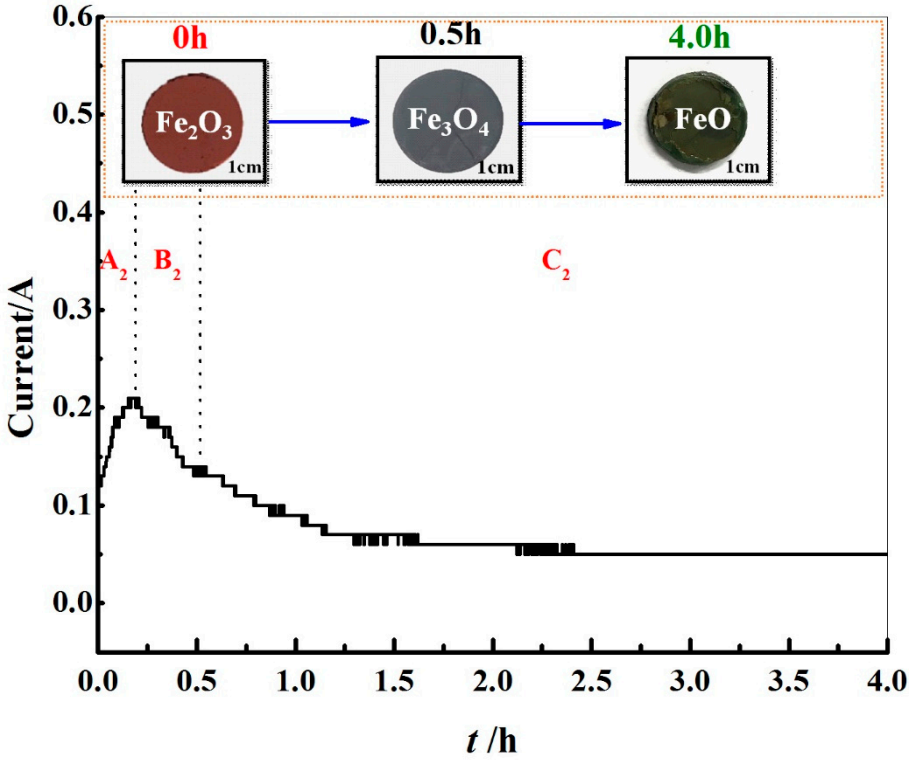

Figure 9. *I–t* curves of electrolysis of S_2 (mFe_2O_3/mAl_2O_3 = 3:2, at 2.3 V, 850 °C, and 4 h).

According to Figures 8 and 9, it can be seen that the reaction from 0 to 0.19 h belonged to stage A, which was an electric double layer charging process. The active particles quickly gathered at 3PIs, and the Fe_2O_3 electro-deoxygenation reaction started at the maximum reaction rate. From 0.19 to 0.75 h, it belonged to stage B, and reaction (2) produced Fe_3O_4, accompanied by the formation of new 3PIs at the junction of Fe_3O_4/Fe_2O_3/NaCl-KCl molten salt. From 0.75 to 4 h, it belonged to stage C, and reaction (3) produced FeO, accompanied by the formation of new 3PIs at the junction of FeO/Fe_3O_4/NaCl-KCl molten salt. It can be seen from Figure 4 that the electro-deoxidation reaction with different Fe_2O_3 contents included three stages, A, B, and C. Combining the results of Figures 8 and 9, the Fe_2O_3/Al_2O_3 electro-deoxidation reaction mechanism could be obtained, as shown in Figure 10. With the increase in the Fe_2O_3 content, the concentration of activated molecules in the system was increased, the resistance of Al_2O_3 in the system was reduced, and the reaction rate of reactions (2) and (3) was increased. This shortened the completion time of stages A, B, and C.

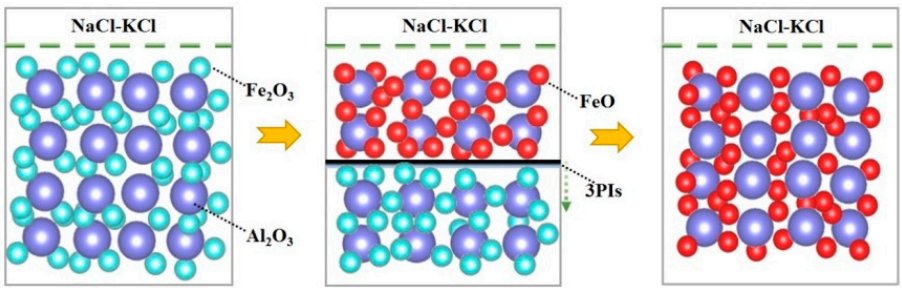

Figure 10. Schematic illustration of electrochemical process during the electro-reduction of Fe_2O_3/Al_2O_3.

4. Conclusions

In this paper, molten salt electrolysis was used to study the reaction process of Fe_2O_3-Al_2O_3 electrolytic reduction of FeO-Al_2O_3 in the NaCl-KCl system. The influence of the

Fe_2O_3 content on the electrolysis process was analyzed. When the electrolysis conditions were 850 °C, 2.3 V, and a reaction time of 4 h, Fe_2O_3-Al_2O_3 could be electrolyzed to Fe_3O_4, FeO, and Al_2O_3. FeO-Al_2O_3 could be obtained by adjusting the content of Fe_2O_3. The increasing content of Fe_2O_3 could increase the rate of the deoxidation reaction and shorten the time of Fe_2O_3 reduction to Fe_3O_4 and Fe_3O_4 reduction to FeO. The electrolysis product nucleated and grew around Al_2O_3, and it finally became angular polyhedrons. By studying the dynamic process of the electro-deoxygenation reaction, the electro-deoxygenation reaction mechanism was obtained. It included electric double layer charging, Fe_2O_3 electro-deoxygenation to produce Fe_3O_4, and Fe_3O_4 electro-deoxygenation to produce FeO, accompanied by the formation of new 3PIs, O^{2-} transport, and other reactions. The principle of obtaining FeO by adjusting the content of Fe_2O_3 was that the increase in the Fe_2O_3 content increased the concentration of activated molecules in the system. Additionally, it reduced the resistance of Al_2O_3 in the system. The active particles migrated more smoothly in the cathode and increased the reaction rate of reactions (2) and (3). The reaction rate shortened the reaction time of the electric double layer charging, Fe_3O_4 generation, FeO generation, and other stages. As we all know, in addition to the Fe_2O_3 content, the reaction temperature, reaction time, and voltage are all factors that affect the electrolytic reduction of Fe_2O_3-Al_2O_3 to FeO-Al_2O_3. Subsequent research will focus on the mechanism of the reaction temperature, reaction time, and voltage in the reduction process.

Author Contributions: Y.X. designed the experiments; Z.J. analyzed the data; H.Y. wrote the paper; X.Q. reviewed the paper; H.L. and J.L. guided the experiment. All authors have read and agreed to the published version of the manuscript.

Funding: This research was funded by the National Natural Science Foundation of China, grant number 51874141.

Institutional Review Board Statement: Not applicable for studies not involving humans or animals.

Informed Consent Statement: Not applicable for studies not involving humans.

Data Availability Statement: Not applicable.

Acknowledgments: This work was supported by the National Natural Science Foundation of China (No. 51874141).

Conflicts of Interest: The authors declare they have no conflict of interest. The funders had no role in the design of the study; in the collection, analysis, or interpretation of data; in the writing of the manuscript; or in the decision to publish the results.

References

1. Khairul, M.A.; Zanganeh, J.; Moghtaderi, B. The composition, recycling and utilization of Bayer red mud. *Res. Cons. Rec.* **2019**, *141*, 483–498. [CrossRef]
2. Fan, G.Q.; Wang, M.; Dang, J.; Zhang, R.; Lv, Z.P.; He, W.C.; Lv, X.W. A novel recycling approach for efficient extraction of titanium from high-titanium-bearing blast furnace slag. *Waste Manag.* **2021**, *120*, 626–634. [CrossRef]
3. Wang, N.; Yan, H.Y.; Luo, C.; Li, H. Thermodynamic analysis of preparation of cermet from zinc kiln slag. In *TMS 2021 11th International Symposium on High-Temperature Metallurgical Processing*; Springer: Cham, Switzerland, 2020; pp. 1023–1032.
4. Agrawal, S.; Dhawan, N. Investigation of carbothermic microwave reduction followed by acid leaching for recovery of iron and aluminum values from Indian red mud. *Miner. Eng.* **2020**, *159*, 106653. [CrossRef]
5. Mancini, A.; Lothenbach, B.; Geng, G.; Grolimund, D.; Wieland, E. Iron speciation in blast furnace slag cements. *Cem. Concr. Res.* **2021**, *140*, 106287. [CrossRef]
6. Geng, C.; Liu, J.; Wu, S.; Jia, Y.; Du, B.; Yu, S. Novel method for comprehensive utilization of MSWI fly ash through co-reduction with red mud to prepare crude alloy and cleaned slag. *J. Hazard. Mater.* **2020**, *384*, 121315. [CrossRef] [PubMed]
7. Mukiza, E.; Zhang, L.L.; Liu, X.; Zhang, N. Utilization of red mud in road base and subgrade materials: A review. *Resour. Conserv. Recycl.* **2019**, *141*, 187–199. [CrossRef]
8. Luo, C.; Peng, J.; Yan, H.Y.; Liang, J.L. Thermodynamic behavior analysis of Fe-$FeAl_2O_4$ cermet prepared by zinc kiln slag. In *TMS 2021 150th Annual Meeting & Exhibition Supplemental Proceedings*; Springer International Publishing: Cham, Switzerland, 2021; pp. 935–942.
9. Ma, T. Preparation of Fe-Al-Based Cermet with Red Mud and Properties Study. Master's Thesis, University of Science and Technology Beijing, Beijing, China, 2017; pp. 52–70.

10. Ikram, U.H.M.; Mukherjee, P.S.; Khanna, R. Formation of light-weight ferroalloys in the Fe_2O_3-Al_2O_3-C system at 1550 C: Influence of silica impurities. *Metals* **2017**, *7*, 391. [CrossRef]
11. Chobtham, C.; Kongkarat, S. Synthesis of hercynite from aluminium dross at 1550 °C: Implication for Industrial Waste Recycling. *Mater. Sci. Forum.* **2020**, *977*, 223–228. [CrossRef]
12. Zhang, R.; Dang, J.; Liu, D.; Lv, Z.P.; Fan, G.Q.; Hu, L.W. Reduction of perovskite-geikielite by methane–hydrogen gas mixture: Thermodynamic analysis and experimental results. *Sci. Total. Environ.* **2020**, *699*, 134355. [CrossRef]
13. Zhou, L.; Enakonda, L.R.; Saih, Y.; Loptain, S.; Basset, J.M. Catalytic methane decomposition over Fe-Al_2O_3. *ChemSusChem* **2016**, *9*, 1243–1248. [CrossRef]
14. Mei, D.; Zhao, H.; Yan, S. Kinetics model for the reduction of Fe_2O_3/Al_2O_3 by CO in chemical looping combustion. *Chem. Eng. Process.-Process Intensif.* **2018**, *124*, 137–146. [CrossRef]
15. Ohno, K.; Konishi, H.; Watanabe, T.; Ishihara, S.; Kunitomo, K. Effect of pre-reduction degree on softening behavior of simulant sinter Iron ore. *ISIJ Int.* **2020**, *60*, 1520–1527. [CrossRef]
16. Chen, G.Z.; Fray, D.J.; Farthing, T.W. Direct electrochemical reduction of titanium dioxide to titanium in molten calcium chloride. *Nature* **2000**, *407*, 361–364. [CrossRef] [PubMed]
17. Pal, U.B.; Woolley, D.E.; Kenney, G.B. Emerging SOM technology for the green synthesis of metals from oxides. *JOM* **2001**, *53*, 32–35. [CrossRef]
18. Ono, K.; Suzuki, R.O. A new concept for producing Ti sponge: Calciothermic reduction. *JOM* **2002**, *54*, 59–61. [CrossRef]
19. Jiao, S.Q.; Zhu, H.M. Novel metallurgical process for titanium production. *J. Mater. Res.* **2006**, *21*, 2172–2175. [CrossRef]
20. Chen, G.Z. Interactions of molten salts with cathode products in the FFC Cambridge Process. *Int. J. Miner. Metall. Mater.* **2020**, *27*, 1572–1587. [CrossRef]
21. Li, H.; Jia, L.; Liang, J.L.; Yan, H.Y.; Cai, Z.Y.; Reddy, R.G. Study on the direct electrochemical reduction of Fe_2O_3 in NaCl-$CaCl_2$ melt. *Int. J. Electrochem. Sci.* **2019**, *14*, 11267–11278. [CrossRef]
22. Pepper, R.A.; Couperthwaite, S.J.; Millar, G.J. Comprehensive examination of acid leaching behaviour of mineral phases from red mud: Recovery of Fe, Al, Ti, and Si. *Miner. Eng.* **2016**, *99*, 8–18. [CrossRef]
23. Heo, J.H.; Chung, Y.; Park, J.H. Recovery of iron and removal of hazardous elements from waste copper slag via a novel aluminothermic smelting reduction (ASR) process. *J. Clean. Prod.* **2016**, *137*, 777–787. [CrossRef]
24. Zhu, X.; Niu, Z.; Li, W.; Zhao, H.; Tang, Q. A novel process for recovery of aluminum, iron, vanadium, scandium, titanium and silicon from red mud. *J. Environ. Chem. Eng.* **2020**, *8*, 103528. [CrossRef]
25. Li, G.; Wang, D.; Chen, Z. Direct reduction of solid Fe_2O_3 in molten $CaCl_2$ by potentially green process. *J. Mater. Sci. Technol.* **2009**, *25*, 767–771.
26. Mohandas, K.S. Direct electrochemical conversion of metal oxides to metal by molten salt electrolysis: A review. *Miner. Process. Extr. Metall.* **2013**, *122*, 195–212. [CrossRef]
27. Xie, Z.P. *Structural Ceramics*; Tsinghua University Press: Beijing, China, 2011; pp. 332–356.